New excitation functions for proton induced reactions on natural gadolinium up to 70 MeV with focus on ^{149}Tb production

R. Formento-Cavaier, Ferid Haddad, C. Alliot, T. Sounalet, I. Zahi

Version of Record: https://www.sciencedirect.com/science/article/pii/S0168583X20303104
Manuscript_723c2e7a3025b4b1670db7edd9e1d81d

New excitation functions for proton induced reactions on natural gadolinium up to 70 MeV, focus on ^{149}Tb production

R. Formento-Cavaier[1,2,3], F. Haddad[2,3], C. Alliot[2,4], T. Sounalet[2,3] and I. Zahi[1]

[1] *Advanced Accelerator Applications, a Novartis company, 20 rue Diesel, 01630 Saint-Genis-Pouilly, France*
[2] *GIP Arronax, 1 rue Aronnax, 44800 Saint Herblain, France*
[3] *Subatech, CNRS/IN2P3, IMT Atlantique, Université de Nantes, CS 20722 44307 Nantes cedex, France*
[4] *Inserm, U892, 1 quai Moncousu, 44 Nantes, France*

ABSTRACT

Terbium is one of the most interesting elements for new potential theranostics applications. Indeed, the physical properties of four of its radionuclides (^{149}Tb, ^{152}Tb, ^{155}Tb, ^{161}Tb) allow their use in each main applications of nuclear medicine. ^{149}Tb is the lowest mass alpha emitter, and the only one among the radiolanthanides, with suitable physical properties for receptor-targeted alpha therapy (TAT). Currently ^{149}Tb is only produced through spallation reactions induced by high-energy proton beam coupled with mass separation to obtain suitable purity. The aim of the present work is to investigate the production of ^{149}Tb using commercial cyclotrons by irradiation of natural gadolinium target. New excitation functions for proton-induced nuclear reactions on natural gadolinium have been measured. Our results extend current knowledge up to 70 MeV and are in good agreement with existing data at low energy. From this new set of data, production yield estimations are calculated and discussed.

1. Introduction

In nuclear medicine, one of the key emerging concepts is the theragnostic approach. It is an integrated medical approach coupling both the diagnostic and therapy modalities. This can be achieved by using the same vector molecule labeled to a different radionuclide for imaging or therapy. Thus, using the same vector for both imaging first and therapy then, allows reaching the target organ in the same way and with the same efficiency. Using the information from the diagnostic agent, the patient response can be inferred as well as the stage of the disease. If the treatment can be applied, a dosimetry study can help defining the best dose to use. After treatment, a follow-up can be performed with eventual additional use of the diagnostic agent.

One of the most interesting elements for future potential theranostics applications is terbium, which offers four radionuclides with suitable characteristics for medical applications: ^{149}Tb ($T_{1/2}$=4.12 h) for targeted alpha therapy, ^{152}Tb ($T_{1/2}$=17.5 h) for PET, ^{155}Tb ($T_{1/2}$=5.32 d) for SPECT (and possibly targeted Auger therapy) and ^{161}Tb ($T_{1/2}$=6.89 d) for targeted β^- therapy. Their main physical properties are summarized in Table 1.

Table 1: Medical terbium radionuclides physical properties. (1)

Radioisotope	**Tb-149**	**Tb-152**	**Tb-155**	**Tb-161**
Half-life	4.12 h	17.5 h	5.32 d	6.89 d
Decay mode	α (16.7%) EC (83.3%)	ε (100%)	EC (100%)	β- (100%)
Main γ emission (keV)	164.9 (26.4%) 352.2 (29.4%) 511 (14.2%)	271.1 (9.5%) 344.3 (63%) 511 (41%)	86.5 (32%) 105.3 (25%)	25.6 (23.2%) 48.9 (17%) 74.6 (10.2%)
Mean/max. β- emission (keV)	N/A	N/A	N/A	138/460 (26%) 157/522 (65%)
α emission (MeV)	3.97 (16.7%)	N/A	N/A	N/A

Nevertheless, apart from ^{161}Tb which can be produced from nuclear reactors, the availability of the three other radionuclides is currently limited to few batches per year from high energies mass separation facilities such as CERN-MEDICIS (2). One method to increase the availability of these isotopes is to consider their production through a commercial accelerator such as a cyclotron. In order to evaluate the yields of ^{149}Tb production from cyclotron, new experimental data are needed. In this work, the cross-section and yield achievable from the irradiation of natural gadolinium with 70 MeV proton beam have been investigated. Furthermore, the production cross section for the other terbium radionuclides, which are co-produced, have been evaluated too.

2. Experimental method

2.1. Stacked foils method

The stacked foils method is a well-known technique used for cross-sections measurements (3). A typical stack is made of several pattern composed of several foils each having a dedicated role (Figure 1):

- *The target foil* is made of the starting material for the investigation of the considered nuclear reaction.
- *The monitor foil* is used to get a measure of the beam current at its location. It is made of an element for which, at least one reaction cross section is well known.
- *The catcher foil* is used to recover the eventual fraction of escaped recoil atoms from the monitor foil. The monitor foil plays the same role for the target foil.
- *The degrader foil* is used to decrease the beam energy before entering the next pattern. The thickness of the foils is thus defined to obtain a suitable number of experimental points

in order to properly describe the investigated excitation function.

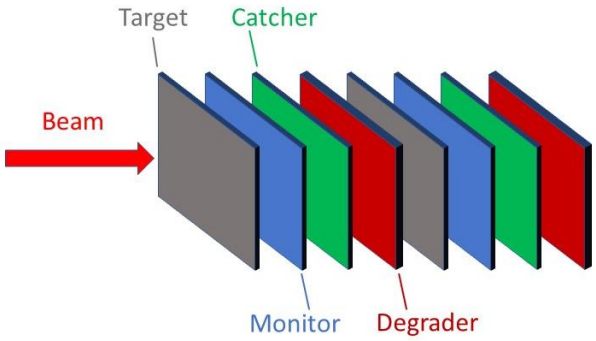

Fig. 1. Stacked foils overview. Example of a typical stack configuration.

The activity of the produced radionuclides in a thin foil (up to a few dozen of µm) can be calculated as follows:

$$A = \phi * \sigma * \frac{X*N_A*\rho_A}{M} * (1 - e^{-\lambda t_{irr}}) \quad (1)$$

Where:

ϕ is the proton beam current in particles/s
σ is the reaction cross section in cm^2
X is the enrichment of the target (%)
N_A is the Avogadro's constant in atoms/mol
ρ_A is the area density of the target in g/cm^2
σ is the molar mass of the target in g/mol
t_{irr} is the irradiation time in s
M is the molar mass of the target element (g/mol)

In order to evaluate the cross section of new investigated reactions, one can use a reference cross section validated by IAEA (4). Those are monitor cross sections validated after numerous cross section measurements of the same reaction by different group of researchers. Therefore, the searched cross section is calculated assuming the beam current of the target foil is equal to the beam current of the monitor foil positioned next to it, as the beam loss of energy in a thin foil is negligible. It is then possible to equalize the expressions of the flux for both the target produced and monitor produced radionuclides (see equation 2). In the following equations the monitor quantities will be denoted with an apex (ex. ϕ').

$$\frac{A*M}{\sigma*X*N_A*\rho_A*(1-e^{-\lambda t_{irr}})} = \frac{A'*M'}{\sigma'*X'*N_A*\rho'_A*(1-e^{-\lambda' t_{irr}})} \quad (2)$$

where the unknown of the equation is only σ, the cross section of the investigated reaction. We can then express the unknown cross section σ as a function of all the above parameters as shown in equation (3):

$$\sigma = \sigma' * \frac{A*M*X'*\rho'_A*(1-e^{-\lambda' t_{irr}})}{X*\rho_A*(1-e^{-\lambda t_{irr}})*A'*M'} \quad (3)$$

The cross section uncertainty is estimated through the propagation error calculation. Since all parameters of equation 3 are independent, the total error is expressed as a quadratic sum and is presented in eq. 4:

$$\frac{\Delta\sigma}{\sigma} = \sqrt{\left(\frac{\Delta\sigma'}{\sigma'}\right)^2 + \left(\frac{\Delta A}{A}\right)^2 + \left(\frac{\Delta A'}{A'}\right)^2 + \left(\frac{\Delta\rho_A}{\rho_A}\right)^2 + \left(\frac{\Delta\rho'_A}{\rho'_A}\right)^2} \quad (4)$$

The main uncertainties come from the measured activities which is less than 10% in most cases and the uncertainty on the recommended cross section values. Since no uncertainties are given for the recommended cross section values, we use the error of the closest experimental points for each measured point. It turns out to be of the order of 10% (5).

2.2. Experimental setup

Three experiments, spread over a period of several months, have been performed at GIP ARRONAX cyclotron (Nantes, FR) (6). The irradiations parameters for these experiments were a beam intensity of 100 nA and an irradiation duration of 30 min resulting in a total integrated current of 50 nAh,

The GIP ARRONAX beam line is under vacuum and closed using a 75 µm thick kapton foil. The stack foils were positioned in air, 7 cm after the kapton foil. The energy loss through each thin foil was determined using SRIM software (7) and the different material crossed by the projectiles. The energy associated to the experimental points was taken in the middle of the target foil. A 0.5 MeV incident beam energy error was considered as described in a previous work performed in the same facility (8).

A typical irradiated stacked is presented in Table 2. Each thin foil was weighed and scanned before irradiation to precisely determine its area. Thus, from these values, the thickness was accurately deduced. Different degrader foil thicknesses were used depending on the desired energy degradation in the stack.

Table 2: Experimental stacked foils composition

Foil	**Material**	**Thickness**
Target	Gadolinium	2 µm
Monitor	Nickel	10 µm
Catcher	Aluminium	10 µm
Degrader	Aluminium	100 to 800 µm

The choice of purchasing very thin gadolinium foils of 2 µm are related to the ^{149}Tb quantification. Indeed, as ^{149}Tb is an alpha emitter with 16.7 % branching ratio, in this work the cross section ^{nat}Gd(p,x)^{149}Tb is estimated from the foil counting in the alpha detector. Due to the dramatic alpha particle loss of energy in the matter, the thickness of the foils should be as thin as possible for quantifying accurately the produced activity of ^{149}Tb. After SRIM simulations, it was found that with 2 µm foils a clear peak must be identified. An example of a

typical spectrum is presented in figure 2. The monitor foil selected was nickel in order to use the reaction producing ^{57}Ni ($T_{1/2}$= 35.6h; reaction: ^{nat}Ni(p,x)^{57}Ni). This reference cross section is given by the IAEA (4).

2.3. Experimental measurements

The ^{149}Tb cross section from natural gadolinium with proton beam between 70 and 58 MeV is the main aim of this work due to the lack of available data. Based on the radiation emitted by the produced radionuclides, we have used alpha spectrometry to determine the activity of ^{149}Tb and gamma spectrometry for all other radionuclides.

2.4. Alpha spectrometry

The results of the alpha spectrometry can be quantified as ^{149}Tb has the most energetic alpha emission among the co-produced detectable radioisotopes, here 3.967 MeV. The list of the alpha emitters potentially co-produced or generated from decay of other produced radionuclides in the considered beam energy range, are reported in Table 3 with their energy and intensity emission.

Table 3: alpha emitters potentially co-produced with a 70-58 MeV proton beam and natural gadolinium target.

Element	Isotope	Half-life	Energy (MeV)	Branching ratio
Terbium	Tb-149	4,12 h	3,967	16,70%
	Tb-149m	4,2 m	3,999	0,02%
	Tb-150	3,48 h	3,492	0,05%
	Tb-151	17,81 h	3,407	0,009%
Gadolinium	Gd-148	71.1 y	3,182	100%
	Gd-149	9.28 d	3,016	0,0004%
	Gd-150	1.76E6 y	2,726	100%
	Gd-151	120 d	2,6	0,00%
Europium	Eu-147	24.1 d	2,908	0,0022%
	Eu-148	54.5 d	2,63	0,00%
Samarium	Sm-146	6.8E7 y	2,46	100%

As shown in Table 3, the other alpha emission contributions are negligible following their emission intensity or the too long half-life. The only emission more energetic than the one of interest is from ^{149m}Tb. It decays 99.98 % ε in ^{149}Gd and 0.02% α in ^{145}Eu. Nevertheless, its half-life is 4.2 minutes. As the first foil measurement is made after 2 hours, the contribution of this radionuclide can be considered negligible both due to its intensity and its decay. Particular attention has been made only on ^{151}Tb emission as its energy is situated in the tail of ^{149}Tb emission, and it smoothly influences the measurement during the last counting, 1 day after EOB. In that case, ^{149}Tb was almost fully decayed and ^{151}Tb was still quite present. For this reason, to calculate the ^{149}Tb activity the detected counts were subtracted by the counts generated by ^{151}Tb, which activity was estimated by gamma spectrometry. In order to prevent any source of error due to a potential contamination of the spectrometer chamber, one measurement of the empty chamber was performed after each last measurement of each experiment, thus the background was subtracted. The effect of those two factors was evident because allowed the consistency of the calculated ^{149}Tb activities along each measurement.

All our measurements have been done using a Passivated Implanted Planar Silicon (PIPS) detector Alpha Series A of Canberra. It has a minimum active thickness greater than 140 µm, which is sufficient for the full absorption of alpha particles of up to 15 MeV. Our detectors have been calibrated using a multi alpha particles source (Am-241, Pu-239, Cm-243) certified by Cerca LEA(France). An example of a spectrum obtained by counting a 2 µm thick irradiated Gd foil is presented in figure 2. We can clearly see a peak with an end-point corresponding to the energy associated to the main alpha emission of ^{149}Tb. The broadening of the peak is mainly coming from the energy loss within the target thickness of alpha particle emitted inside the target foil.

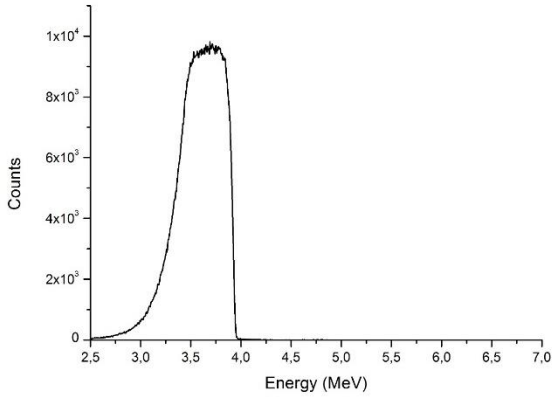

Fig. 2: alpha spectrometry spectrum obtained from the measurement of a 2 µm gadolinium foil.

2.6 Gamma spectrometry

The terbium radionuclides produced from the natural gadolinium target present a large number of gamma ray emission, often at the same or close energy of other emission from other produced radionuclides. For this reason, all the produced radionuclides had to be identified. For that purpose, we used the FitzPeaks software for peak search, fitting and activity determination whereas we calculate the activity error from hand calculations. For some radionuclides, interferences occur and we have considered this effect by subtracting the activity of other radionuclides defined using other gamma rays available. The nuclear data used for the investigated radionuclides are listed in Table 4. They are all the co-produced terbium contaminants. Other element's radionuclides are co-produced and were identified. However, as they can be chemically separated, we don't need their quantification. For the evaluation and comparison of the gamma rays, two databases were used: NNDC database (1) and the Lund/LBNL Nuclear Data Search (9). When the two databases were in disagreement, priority was given to NNDC.

Table 4: Gamma ray energies and intensities used for the quantification of the activity of the listed radionuclides.

Radionuclide	Half-life	Energy (keV)	Intensity (%)
Tb-150	3.48 h	638	72
		496	14,6
Tb-151	17.61 h	251,86	26,3
		287,35	28,3
Tb-152	17.5 h	271,13	8,6
		344,27	65
		586,26	9,4
Tb-153	2.3 d	212	31
Tb-154	21 h	1291,3	6,9
		1123	6,1
Tb-154m	22.7 h	225,9	26,8
Tb-155	5.32 d	180	7,45
		367	1,48
Tb-156	5.35 d	199,21	40,9
		356,42	13,6
		534,32	66,6

An example of a spectrum obtained during one gamma spectrometry measurement is given in figure 3.

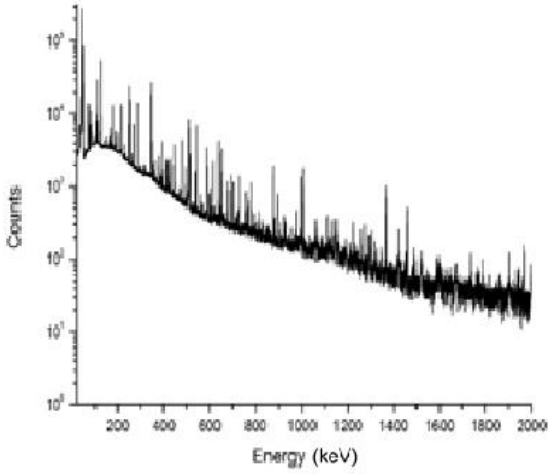

Fig. 3: Gamma spectrum of one natural Gd foil obtained during our experiment.

2.7. Reactions

In Table 5 are listed the nuclear reactions, and associated energy threshold, concurring for the production of the considered radionuclides.

Table 5: Nuclear reaction and associated threshold energy of the considered reactions.

RN	Half-life	Reaction	Threshold energy (MeV)
Tb-149	4.12 h	^{152}Gd(p,4n)^{149}Tb	28.4
		^{154}Gd(p,6n) ^{149}Tb	43.6
		^{155}Gd(p,7n) ^{149}Tb	50.1
		^{156}Gd(p,8n) ^{149}Tb	58.7
		^{157}Gd(p,9n) ^{149}Tb	65.1
Tb-150	3.48 h	^{152}Gd(p,3n)^{150}Tb	20.6
		^{154}Gd(p,5n) ^{150}Tb	35.9
		^{155}Gd(p,6n) ^{150}Tb	42.3
		^{156}Gd(p,7n) ^{150}Tb	50.9
		^{157}Gd(p,8n) ^{150}Tb	65.3
Tb-151	17.61 h	^{152}Gd(p,2n) ^{151}Tb	12.0
		^{154}Gd(p,4n) ^{151}Tb	27.2
		^{155}Gd(p,5n) ^{151}Tb	33.7
		^{156}Gd(p,6n) ^{151}Tb	42.3
		^{157}Gd(p,7n) ^{151}Tb	48.7
		^{158}Gd(p,8n)^{151}Tb	56.7
Tb-152	17.5 h	^{152}Gd(p,n)^{152}Tb	4.8
		^{154}Gd(p,3n)^{152}Tb	20.0
		^{155}Gd(p,4n) ^{152}Tb	26.5
		^{156}Gd(p,5n) ^{152}Tb	35.1
		^{157}Gd(p,6n) ^{152}Tb	41.5
		^{158}Gd(p,7n) ^{152}Tb	49.5
		^{160}Gd(p,9n) ^{152}Tb	62.9
Tb-153	2.3 d	^{152}Gd(p,γ)^{153}Tb	0
		^{154}Gd(p,2n) ^{153}Tb	11.3
		^{155}Gd(p,3n) ^{153}Tb	17.8
		^{156}Gd(p,4n) ^{153}Tb	26.4
		^{157}Gd(p,5n) ^{153}Tb	32.8
		^{158}Gd(p,6n) ^{153}Tb	40.7
		^{160}Gd(p,8n) ^{153}Tb	54.2
Tb-154	21 h	^{154}Gd(p,n) ^{154}Tb	4.3
		^{155}Gd(p,2n) ^{154}Tb	10.8
		^{156}Gd(p,3n) ^{154}Tb	19.4
		^{157}Gd(p,4n) ^{154}Tb	25.8
		^{158}Gd(p,5n)^{154}Tb	33.8
		^{160}Gd(p,7n)^{154}Tb	47.2
Tb-155	5.32 d	^{154}Gd(p,γ)^{155}Tb	0
		^{155}Gd(p,n) ^{155}Tb	1.6
		^{156}Gd(p,2n) ^{155}Tb	10.2
		^{157}Gd(p,3n) ^{155}Tb	16.6
		^{158}Gd(p,4n) ^{155}Tb	24.6
		^{160}Gd(p,6n) ^{155}Tb	38.0
Tb-156	5.35 d	^{155}Gd(p,γ)Tb^{156}	0
		^{156}Gd(p,n)Tb^{156}	3.2
		^{157}Gd(p,2n)Tb^{156}	9.6
		^{158}Gd(p,3n)Tb^{156}	17.6
		^{160}Gd(p,5n)Tb^{156}	31.1

3. Results

The cross section values obtained as a function of the incident proton beam energy, using eq. 3 and their error using eq. 4, during the whole experimental campaign are given in Table 6, Table 7 and Table 8 and explained in the next paragraphs.

Table 6: Cross section values obtained in this work for the production of Tb-149 by alpha spectrometry (uncertainty with k=1).

Energy (MeV)	*Cross section Tb-149 (mb)*
69.83 ± 0.51	*7.11 ± 0.72*
68.11 ± 1.13	*6.89 ± 0.69*
66.37 ± 1.64	*5.69 ± 0.57*
65.40 ± 0.79	*5.00 ± 0.50*
64.59 ± 2.26	*4.42 ± 0.44*
64.26 ± 1.21	*4.89 ± 0.49*
63.82 ± 0.58	*4.67 ± 0.47*
63.11 ± 1.64	*3.74 ± 0.37*
61.98 ± 1.11	*3.62 ± 0.36*
60.05 ± 1.64	*2.14 ± 0.22*
58.08 ± 2.55	*1.45 ± 0.15*

Table 7: Cross section values obtained in this work for the production of ^{150}Tb, ^{151}Tb, ^{152}Tb and ^{153}Tb using gamma spectrometry (uncertainty with k=1).

Energy (MeV)	*Cross sections Tb-150 (mb)*	*Tb-151 (mb)*	*Tb-152 (mb)*	*Tb-153 (mb)*
58.2 ± 2.5	*21.0 ± 2.1*	*95.8 ± 9.8*	*122.3 ± 12.3*	*171.3 ± 17.4*
60.1 ± 1.6	*18.3 ± 1.9*	*83.9 ± 8.9*	*118.4 ± 12.0*	*148.3 ± 14.9*
62.0 ± 1.1	*22.6 ± 2.3*	*100.6 ± 10.4*	*118.0 ± 11.6*	*164.7 ± 17.2*
63.8 ± 0.6	*27.3 ± 2.8*	*106.5 ± 10.8*	*119.5 ± 13.2*	*167.5 ± 19.3*
63.1 ± 1.6	*23.3 ± 2.4*	*105.0 ± 11.3*	*124.0 ± 14.1*	*159.0 ± 16.2*
64.3 ± 1.2	*26.9 ± 2.7*	*108.1 ± 10.9*	*121.9 ± 12.3*	*167.6 ± 17.3*
65.4 ± 0.8	*20.7 ± 2.4*	*98.0 ± 10.0*	*115.3 ± 11.9*	*146.0 ± 14.8*
66.4 ± 1.6	*26.4 ± 2.7*	*107.6 ± 10.9*	*118.3 ± 11.9*	*146.7 ± 14.8*
68.1 ± 1.1	*28.3 ± 2.9*	*102.3 ± 10.4*	*117.9 ± 11.9*	*137.8 ± 14.0*
69.8 ± 0.5	*30.8 ± 3.1*	*96.0 ± 9.9*	*114.0 ± 11.5*	*123.9 ± 12.9*

Table 8: Cross section values obtained in this work for the production of ^{154}Tb, ^{154m2}Tb, ^{155}Tb and ^{156}Tb using gamma spectrometry (uncertainty with k=1).

Energy (MeV)	*Cross Sections Tb-150 (mb)*	*Tb-151 (mb)*	*Tb-152 (mb)*	*Tb-153 (mb)*
58.2 ± 2.5	*32,9 ± 5,1*	*9,5 ± 1,4*	*152,4 ± 15,9*	*68,8 ± 8,0*
60.1 ± 1.6	*29,6 ± 3,3*	*10,4 ± 1,7*	*117,1 ± 12,2*	*59,8 ± 6,0*
62.0 ± 1.1	*34,1 ± 4,1*	*9,3 ± 1,7*	*146,9 ± 15,7*	*67,0 ± 7,3*
63.8 ± 0.6	*32,8 ± 3,3*	*9,5 ± 1,3*	*137,3 ± 14,0*	*55,7 ± 5,9*
63.1 ± 1.6	*31,7 ± 4,5*	*11,5 ± 1,7*	*138,4 ± 14,1*	*61,5 ± 7,4*
64.3 ± 1.2	*38,2 ± 6,0*	*10,7 ± 1,1*	*130,4 ± 13,6*	*60,6 ± 7,3*
65.4 ± 0.8	*34,5 ± 4,4*	*12,1 ± 1,3*	*115,3 ± 12,9*	*56,3 ± 6,0*
66.4 ± 1.6	*45,6 ± 6,5*	*11,7 ± 1,3*	*135,3 ± 14,0*	*59,7 ± 6,3*
68.1 ± 1.1	*45,5 ± 9,0*	*10,8 ± 1,2*	*134,6 ± 15,1*	*54,0 ± 6,3*
69.8 ± 0.5	*35,3 ± 5,0*	*10,9 ± 1,4*	*114,8 ± 11,8*	*48,7 ± 5,1*

3.1. Tb-149 cross section

As represented in figure 4, results of the three performed experiments are in good agreement within each other, describing the cross section curve in the considered energy range.

Few experimental data are available in literature for the cross section of the reaction natGd(p,x) ^{149}Tb. Mironov *et al* (10) studied this reaction with a proton beam of a 1.1 GeV. The beam was degraded down to 60 MeV resulting in large error bars in the lower energies considered, due to the large energy degradation. The values used for comparison in this work are taken from Janis 4.0 database in the section proton induced reaction, EXFOR data (11).

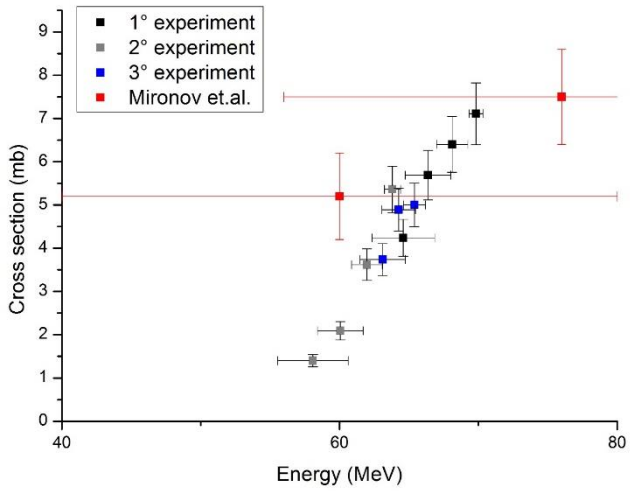

Fig.4. ^{nat}Gd(p,x)^{149}Tb cross section measurement

In figure 5, which is plotted with a larger energy range as the previous figure, we can see that our data clearly fit in the trend defined by the data from Mironov *et al*.

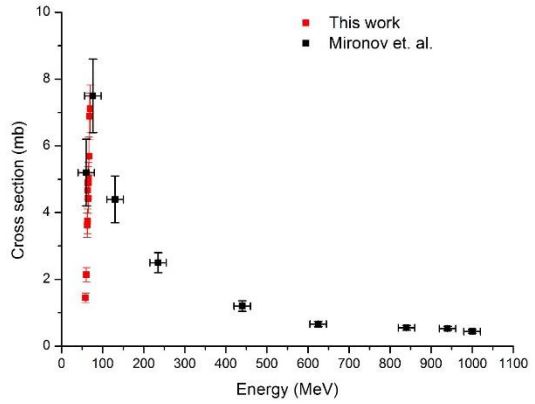

Fig.5. ^{nat}Gd(p,x)^{149}Tb cross section measurement compared to Mironov *et al*.

3.2. Tb-151 cross section

^{151}Tb (half-life 17.6 h) decays 99.991% ε in Gd-151 and 0,009% α in ^{147}Eu. In addition to the ground state, one metastable state (half-life 25 s) is also produced. The metastable state decays rapidly to the ground state by internal transition with branching ratio 93.4 %, and to Gd-151 through ε decays 6.6 %. Due to the short half-life of the metastable state only the cumulative cross section for the production of the ground state can be measured.

The experimental results compared to the curve presented by Vermeulen et al. (12) is shown in the figure 6.

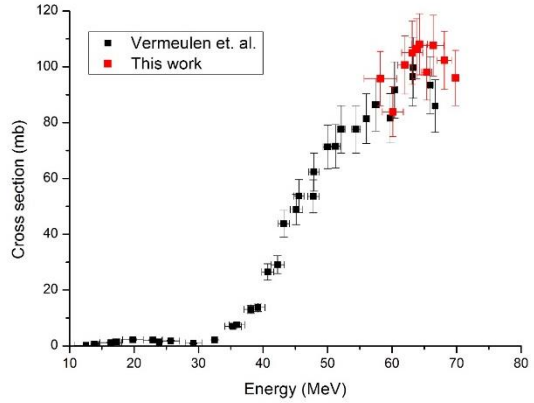

Fig.6. ^{nat}Gd(p,x)^{151}Tb cross section measurement compared to Vermeulen *et al*.

As for ^{149}Tb, we found a good agreement between our three different measurements and a good agreement with the existing data. This gives us some confidence on the quality of our measurements.

3.3. Tb-152 cross section

^{152}Tb (half-life 17.5 h) decays almost 100 % ε in ^{152}Gd and 7E-7% α in ^{148}Eu. In addition to the ground state, one metastable state (half-life 4.2 m) is also produced. It decays to the ground state by internal transition with branching ratio 78.8 %, and to ^{152}Gd through ε decays 21.2 %. Due to the short half-life of the metastable state, only the cumulative cross section for the production of the ground state can be measured as previously.

The experimental results compared to the curve presented by Vermeulen *et al* is shown in Figure 7. Challan *et al* (13) investigated the production of ^{152}Tb too. However, their study was based on proton beam up to 18 MeV, which is very far from this work and compared to the values above 30 MeV that part of the curve corresponds to very low values. This is mainly due to the low natural abundance of ^{152}Gd and ^{154}Gd.

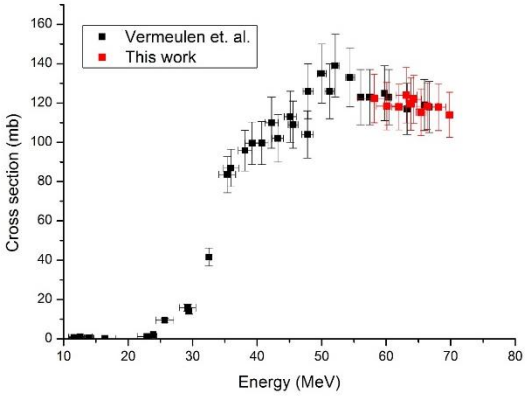

Fig.7. ^{nat}Gd(p,x)^{152}Tb cross section measurement compared to Vermeulen *et al*.

Once more, our data are in perfect agreement with that of the available data in the energy range of interest.

3.4. Tb-153 cross section

^{153}Tb (half-life 2.34 d) decays 100 % through electronic conversion in ^{153}Gd and it has no associated metastable state.

In Figure 8, it is possible to see the good agreement between the experimental points of this work and the curve obtained by Vermeulen *et al*. All the experimental points are in the error bars of the other work values.

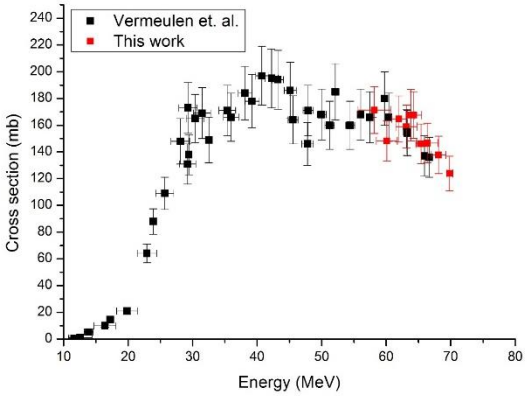

Fig.8. ^{nat}Gd(p,x)^{153}Tb cross section measurement compared to Vermeulen *et al*.

3.5. Tb-154 cross section

^{154}Tb (half-life 21.5 h) decays prevalently ε, almost 100 % in ^{154}Gd, and less than 0.1 % β- in ^{154}Dy (very long-lived alpha emitter). It has two metastable states, which order depends on the database of reference. In this work, they are considered as follow: m1 (half-life 9.4 h) which decays ε with BR around 78.2 %, IT around 21.8% and less than 0.1 % β-; m2 (half-life 22.7 h) which decays ε with a BR 98.2 % and IT 1.8%. For evaluating the gamma rays of the metastable states, only LBNL database has been used as NNDC database reports only gamma ray emission of the ground state. Those three levels have very similar and often have the same gamma ray emissions, therefore they have been evaluated by the very few unique gamma rays. For the ground state, the cumulative cross section has been presented in Figure 9. In the literature, no data have been found for this reaction, whereas Vermeulen *et al* presented the ^{154m2}Tb cross section, which is compared with the experimental points obtained in this work in Figure 10. ^{154m1}Tb was detected by the gamma ray at 540 keV but the high uncertainty associated to this peak activity leads us to not present these results.

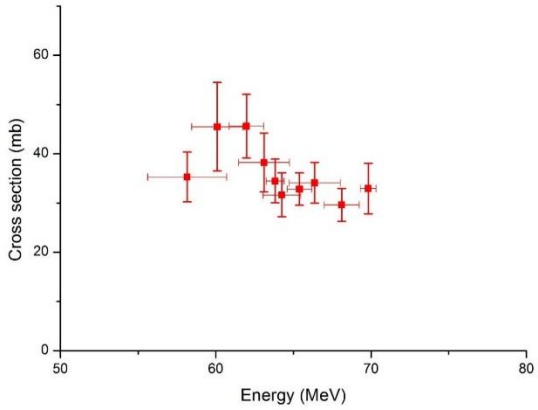

Fig.9. ^{nat}Gd(p,x)^{154}Tb cross section measurement.

As for the cumulative cross section of ^{154}Tb ground state there are no available comparison, only the experimental points obtained in this work are presented.

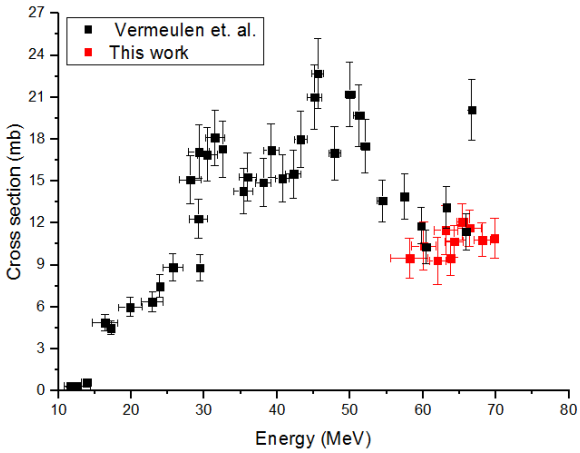

Fig.10. ^{nat}Gd(p,x)^{154m2}Tb cross section measurement compared to Vermeulen *et al*.

For the ^{154m2}Tb cross section, the obtained values are coherent with the ones obtained by Vermeulen *et al*. The point at the highest energy of Vermeulen *et al* data set, which do not follow the behavior of the other data points, is the only one far away from both data sets; nevertheless, it is at an energy value very close to the points in agreement.

3.6. Tb-155 cross section

^{155}Tb (half-life 5.32 d) decays 100% through electronic conversion in ^{155}Gd and it has no associated metastable state. The experimental results compared to the curve presented by Vermeulen *et al* is shown in the figure 11. Good agreement between the experimental data points of this work and the curve obtained by Vermeulen *et al*. can be verified.

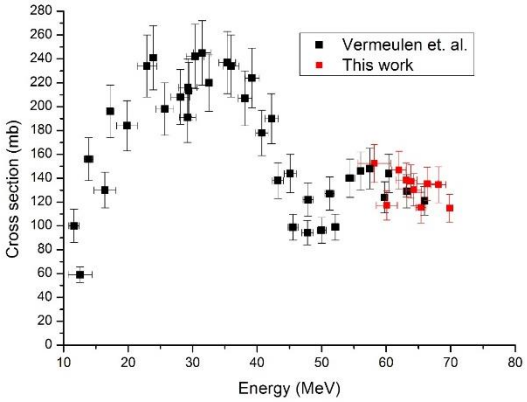

Fig.11. ^{nat}Gd(p,x)^{155}Tb cross section measurement compared to Vermeulen *et al*.

3.7. Tb-156 cross section

^{156}Tb (half-life 5.35 d) decays 100 % ε in ^{156}Gd. It has two metastable states: m1 (half-life 24.4 h) and m2 (half-life 5.3 h) which decays through IT to the ground state. Although, they have a half-life allowing their detection, they emit very low energy and low intensity gamma rays, lower than 90 keV. Therefore, they are quite impossible to detect with accuracy due to the very high background and the large uncertainty in that range of energy. For this reason, only the cumulative cross section for the ground state radionuclide has been evaluated after one to two weeks from EOB.

The experimental results compared to the curve presented by Vermeulen *et al* is shown in the figure 12.

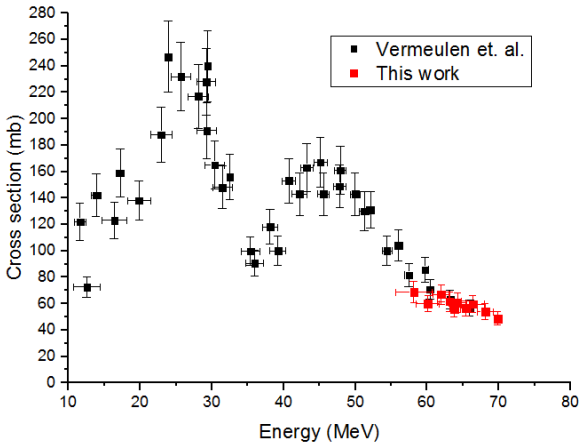

Fig.12. natGd(p,x)^{156}Tb cross section measurement compared to Vermeulen *et al*.

3.8. Tb-150 cross section

^{150}Tb (half-life 3.48 h) decays almost 99.95% ε and 0.05% α. Currently no experimental data have been found in the literature and in databases to compare with our experimental point obtained for the reaction ^{nat}Gd(p,x)^{150}Tb. The activity of ^{150}Tb has been determined using the two peaks at 496 keV (14,6%) and 638 keV (72%). To the total counts obtained analyzing the spectrum, the following contribution have been subtracted to the integrated area of the peaks (uncertainty with k=1):

- Peak 496 keV: Tb-151 (0,3%), Tb-152 (0,1%)
- Peak 638 keV: Tb-151 (0,023%), Tb-153 (0,2%)

This can be accurately determined as the radionuclides emitting interference gamma rays have been quantified with unique gamma as it was shown in previous paragraphs of this article. The two databases used in this work were not in agreement for the gamma ray intensities of ^{150}Tb. Indeed, on LBNL intensities were a factor 100 lower than the one in NNDC. For this reason, only NNDC database was considered for ^{150}Tb.

^{150}Tb has a metastable state which has a very short half-life (5.8 m) hindering his detection. It decays ε in ^{150}Gd.

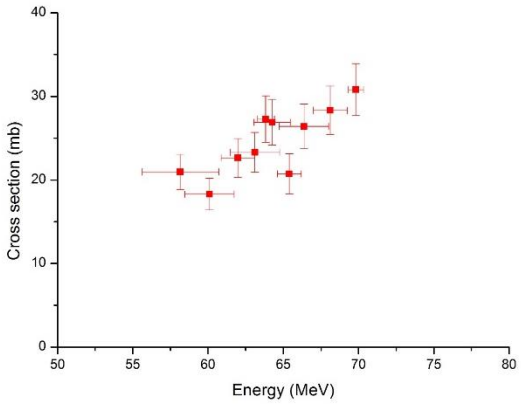

Fig.13. ^{nat}Gd(p,x)^{150}Tb cross section measurements.

4. Thick target yield

Considering the cross section values obtained in this work for ^{149}Tb, a thick target yield estimation has been performed with the software Radionuclide Yield Calculator (RYC) (14). The considered energy window is between 69.8 MeV and 58.2 MeV. Thus, it corresponds to a gadolinium target thickness of 2.74 mm. The thick target yield is 40 MBq/µAh. The integrated yield curve in the considered region is shown in figure 14.

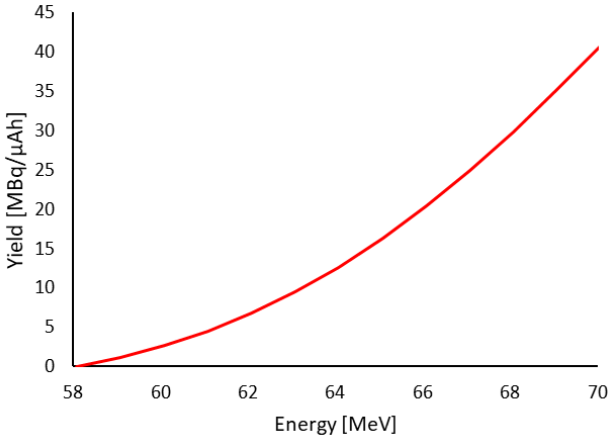

Fig.14. natGd(p,x)^{149}Tb integrated yield

Considering 50 µA of 70 MeV proton beam, and a 10 hours irradiation, the potential yield is 20 GBq at EOB. One way to increase the production yield is to consider enriched gadolinium targets irradiation, (15).

5. Discussion and future perspectives

The aim of this work was to confirm the few experimental data available on the cross section of terbium radionuclides production from natural gadolinium target, and to give new values when applicable. This will allow elaborating a thorough production estimation as well as contaminants estimation verifying whether natural gadolinium can be a suitable starting material or enriched material is best indicated. The overall cross section measurement of the other terbium radionuclides, in particular the interesting ^{152}Tb and ^{155}Tb, confirmed the values already present in literature. Other cross section has been given for the first time to our knowledge, as the one for the cumulative production of ^{150}Tb and ^{154}Tb. Starting from the experimental data, an integral yield of 40 MBq/µAh has been determined for a 2.74 mm thick natural gadolinium target irradiation using 70 MeV proton beam. This confirms the possibility to use commercial cyclotron to produce ^{149}Tb opening the way of a large-scale availability of this isotope. However, the interest of the enriched targets is confirmed for the future potential commercialization of the radionuclide.

Acknowledgments

This research project has been supported by a Marie Skłodowska-Curie innovative training network fellowship of the European commission's horizon 2020 program under contract number 642889 MEDICIS-PROMED.

This work has been, in part, supported by a grant from the French National Agency for Research called "Investissements d'Avenir", Equipex Arronax-Plus noANR-11-EQPX-0004, Labex IRON noANR-11-LABX-18-01and ISITE NExT no ANR-16-IDEX-007.

References

[1]. National Nuclear Data Center (NNDC), Brookhaven National Laboratory, visited on the 30th of November 2018, https://www.nndc.bnl.gov/nudat2/

[2]. R. Augusto, L. Buehler, Z. Lawson, S. Marzari, M. Stachura, T. Stora, CERN-MEDICIS (Medical Isotopes Collected from ISOLDE): A New Facility, Applied Science, 4 (2014) 265-281

[3]. G. Blessing, W. Bräutigam, H.G. Böge, N. Gad, B. Scholten, S.M. Qaim, Appl. Radiat. Isot. 955 (1995) 46–49.

[4]. A. Hermanne *et al*., IAEA monitor reactions 2017, Nuclear Data Sheets 148 (2018) 338-382

[5]. C. Duchemin, A. Guertin, F. Haddad, N. Michel, V. Mëtivier, Production of medical isotopes from a thorium target irradiated by light charged particles up to 70 MeV, Phys. Med. Biol. 60 (2015) 931–946.

[6]. F. Poirier, S. Girault, S. Auduc, C. Huet, E. Mace, J.L. Delvaux, F. Haddad The C70 ARRONAX And Beam Lines Status,Proceedings of IPAC2011, 2011

[7]. J. F. Ziegler. The stopping of energetic light ions in elemental matter, J. Appl. Phys / Rev. Appl. Phys., 85 (1999) 1249–1272

[8]. E. Garrido, C. Duchemin, A. Guertin, F. Haddad, N. Michel, V. Métivier, New excitation functions for proton induced reactions on natural titanium, nickel and copper up to 70 MeV, Nuclear Instruments and Methods in Physics Research B, 383 (2016) 191–212

[9]. S.Y.F. Chu, L.P. Ekström, R.B. Firestone, The Lund/LBNL Nuclear Data Search, Version 2.0, February 1999

[10]. Y. T. Mironov, Features of investigation excitation function of nuclear reactions on internal beam synchrocyclotron, Conf. Nucl. Spectrosc. Nucl. Struct, 9 (2001) 276

[11]. NEA, Java-based Nuclear Data Information System, https://www.oecd-nea.org/janis/, visited on 09/2018

[12]. C. Vermeulen, G.F. Steyn, F. Szelecsényi, Z. Kovacs, K. Suzuki, K. Nagatsu, T. Fukumura, A. Hohn, T.N. van der Walt, Cross-sections of proton-induced reactions on natGd with special emphasis on the production possibilities of Tb152 and Tb155, Nuclear Instrument and Methods in Physics Research B, 275 (2012) 24-32

[13]. M.B. Challan, G.S. Moawad, M.A. Abou-Zeid, M.N.H. Comsan, Excitation Functions of Radionuclides Produced by Proton Induced Reactions on Gadolinium Target, 6th Conference on Nuclear and Particle Physics, 2007

[14]. M. Sitarz, E. Nigron, A. Guertin, F. Haddad and T. Matulewicz, New Cross-Sections for natMo(α,x) Reactions and Medical 97Ru Production Estimations with Radionuclide Yield Calculator, Instruments, 3(1) (2019) 7

[15]. R. Formento Cavaier, F. Haddad, T. Sounalet, T. Stora, I. Zahi, Terbium Radionuclides for Theranostics Applications: A Focus On MEDICIS-PROMED, Physics Procedia 90 (2017) 157-163,